Journal of Advanced Ceramics
2023, **12**(9): 1731–1741
https://doi.org/10.26599/JAC.2023.9220782
ISSN 2226-4108
CN 10-1154/TQ

Research Article

Cyan-green-emitting $Ca_3Sc_2Si_3O_{12}:Ce^{3+}$ transparent ceramics: A promising color converter for high-brightness laser lighting

Huajun Wu[a], Hao Wu[a], Guo-Hui Pan[a], Liangliang Zhang[a], Zhendong Hao[a,*], Jiahua Zhang[a,b,*]

[a]*State Key Laboratory of Luminescence and Applications*, *Changchun Institute of Optics*, *Fine Mechanics and Physics*, *Chinese Academy of Sciences*, *Changchun 130033*, *China*
[b]*Center of Materials Science and Optoelectronics Engineering*, *University of Chinese Academy of Sciences*, *Beijing 100049*, *China*

Received: May 5, 2023; Revised: June 8, 2023; Accepted: June 24, 2023

Abstract: Transparent phosphor ceramics have received increasing attention for high-brightness laser lighting, but commercially available phosphor ceramics are currently mainly limited to yellow YAG:Ce and green LuAG:Ce garnets, leaving a "cyan cavity" which is an obstacle to realizing full-color lighting. Achieving new phosphor ceramics capable of filling the cavity is a challenge. Herein, for the first time, cyan-green-emitting $Ca_3Sc_2Si_3O_{12}:Ce^{3+}$ (CSS:Ce) transparent ceramics have been successfully developed by two-step sintering technique under vacuum. The as-prepared CSS:Ce ceramics present high relative density of 99.7% and optical transmittance of 71% in the cyan-green spectral region. It exhibits an efficient band emission peaking at 504 nm (under 450 nm excitation) with internal/external quantum efficiency of 91%/62%. Furthermore, it has excellent thermal stability with a thermal quenching temperature ($T_{0.5}$) of 838 K, approximately 100 K higher than that of LuAG:Ce ceramics (738 K). In addition, the CSS:Ce ceramics can withstand blue laser density of 45.6 W/mm^2 and meanwhile generates cyan-green light with a forward luminous flux of 813 lm and forward luminous efficacy of 162 lm/W. The CSS:Ce transparent ceramics exhibit excellent luminescence performance comparable to the commercial LuAG:Ce ceramics and could be a highly promising color converter for high-brightness laser lighting.

Keywords: transparent ceramics; color converter; laser lighting; garnet; $Ca_3Sc_2Si_3O_{12}$ (CSS)

1 Introduction

With rapid development of solid-state lighting technology, lamps pumped by high-brightness laser diodes (LDs) are considered to be the next-generation lighting source in some specific areas (including automotive headlights, outdoor lighting, and laser cinema projectors), and they would replace a traditional xenon lamp or a high-pressure sodium lamp (HPSL) [1–5]. However, a traditional color converter is comprised of phosphors, and silicone resin is not applicable to high-brightness laser lighting devices, because resin has poor resistance to heat and high-power-density laser irradiation [6–8]. To overcome weaknesses of organic silicone, several

* Corresponding authors.
E-mail: Z. Hao, haozd@ciomp.ac.cn;
J. Zhang, zhangjh@ciomp.ac.cn

all-inorganic color converters, such as phosphors in glass (PiG), PiG films, single crystals, and phosphor ceramics, have been extensively investigated [9–17]. Among them, phosphor ceramics are recognized to be the most promising color converter for high-brightness solid-state lighting due to their excellent resistance to laser irradiation and thermal shock and easy control of microstructures [18–22]. To date, most laser lighting devices are still involving opaque phosphor ceramics and thus operating in a reflective mode [23,24]. However, encapsulation schemes are complicated, and the tunability of the optical performance is difficult to satisfy different applications. In contrast, the transmissive mode using the transparent ceramics would favor the optic design of the lighting source and the tuning of the resulting optical performance [25–27]. Therefore, it is essential to develop novel transparent phosphor ceramics to be used in the transmissive configuration.

Multicolor-emitting transparent ceramics such as green $Lu_3Al_5O_{12}:Ce^{3+}$ (LuAG:Ce), yellow $Y_3Al_5O_{12}:Ce^{3+}$ (YAG:Ce) and $Gd_3Al_2Ga_3O_{12}:Ce^{3+}$ (GAGG:Ce), red $CaAlSiN_3:Eu^{2+}$, $M_2Si_5N_8:Eu^{2+}$, and $Mg_2Al_4Si_5O_{18}:Eu^{2+}$ have been developed [28–36]. Most of these transparent ceramics exhibit luminescence in the yellow/red spectral region, and a few studies have focused on green–yellow converters such as LuAG:Ce ceramics (peaking at 516 nm) and $Y_3Al_2Ga_3O_{12}:Ce^{3+}$ ceramics (peaking at 525 nm) [37–39]. However, these phosphor ceramics show weak cyan emission and leave a wide "cyan cavity" (460–520 nm) in the emission spectra of laser lighting sources [30–43]. Till now, only yellow YAG:Ce and green LuAG:Ce ceramics are commercially available for high-brightness laser lighting due to their highly efficient emission and excellent resistance to high power density laser irradiation. In terms of full-color laser lighting, the development of highly efficient transparent phosphor ceramics with rich cyan emitting components is thus in demand [44–46].

A cubic $Ca_3Sc_2Si_3O_{12}:Ce^{3+}$ (CSS:Ce) silicate garnet phosphor has drawn much attention for light-emitting diode (LED) lighting due to its compelling optical performance [47–50]. Firstly, CSS:Ce exhibits a further blue-shift emission band in the cyan-green spectral region with a peak at 505 nm compared to green-emitting LuAG:Ce. This enables CSS:Ce a promising candidate for filling the "cyan cavity", providing white light with a relatively high color rendering (Ra $\geqslant$ 85). Secondly, a small Stokes shift between blue and cyan-green favors the reduction of heat generation during the downshifting emission processes. Thirdly, CSS:Ce has excellent chemical and thermal stability, for instance, its emission intensity can remain 60% at 600 K, whereas popular YAG:Ce phosphors drop to 30% [51]. These fascinating luminescence properties of the CSS:Ce phosphor indicate that CSS:Ce transparent ceramics could be a promising color converter for full-color laser lighting if the transparent ceramics could be successfully fabricated.

Unfortunately, the densification of the CSS:Ce ceramics remains a challenge. Compared with the high sintering temperature (~1800 ℃) of YAG and LuAG aluminate garnet ceramics, the sintering process of silicate garnet ceramics must be carried out at a relatively low temperature below its melting point (~1550 ℃). The lower sintering temperature would inhibit lattice diffusion of Ca^{2+} and Sc^{3+} cations during sintering, which is considered as the rate-limiting process of CSS densification. Recently, the ultra-high pressure sintering up to 10 GPa and 1400 ℃ was employed by Irifune *et al*. [52] to realize the densification of $Ca_3Al_2Si_3O_{12}$. Apparently, rigorous synthetic conditions would be a major limitation in large-scale production.

In this work, we report, for the first time, cyan-green-emitting CSS:Ce transparent ceramics via two-step sintering (TSS) technique to realize the full densification of the CSS:Ce ceramics under vacuum. The microstructure, crystalline phase, optical transmittance and luminescence properties were investigated in detail. Furthermore, laser lighting devices were assembled by combining the prepared transparent ceramics with blue LD, and their luminous performance was measured to evaluate their applicability as color converters in laser lighting. The results indicate that the the CSS:Ce transparent ceramics are a promising candidate for high-brightness laser lighting.

2 Experimental

2.1 Fabrication of CSS:Ce transparent ceramics

Commercial available high-purity CaO (Aladdin, China, 99.99%), Sc_2O_3 (Aladdin, China, 99.99%), SiO_2 (Aladdin, China, 99.99%), and CeO_2 (Aladdin, China, 99.99%) were used as starting materials. They were weighted precisely according to the stoichiometric ratio of $Ca_{3-x}Ce_xSc_2Si_3O_{12}$ (x = 0.3%, 0.5%, 0.7%, 0.9%). A small amount of Gd_2O_3 (Aladdin, China,

99.99%) was added as a sintering aid. The mixtures were ball milled for 10 h in ethanol with high-purity ZrO_2 balls. The slurries were dried at 80 ℃ in an oven (DGG-9140AD, Shanghai Senxin Experimental Instrument Co., Ltd., China) for 24 h and sieved through a 200 mesh screen. After that, the powders were uniaxially pressed at 20 MPa into disks and cold isostatic pressed at 200 MPa for 10 min. The green compacts were then sintered using TSS schedules. Typically, the samples were heated at 5 ℃/min to a higher temperature of 1500 ℃ without soaking time, and then immediately cooled at 10 ℃/min to a lower temperature of 1450 ℃ for isothermal sintering and held for 6 or 10 h. To compare with TSS, single-step conventional sintering and zero-time sintering were performed at temperatures of 1450 and 1500 ℃, respectively. For conventional sintering, the samples were heated to 1450 ℃ and held for 10 h. For zero-time sintering, the samples were heated to 1500 ℃ and immediately cooled down to room temperature. The whole sintering process was conducted under high vacuum (1.0×10^{-4} Pa) in a tungsten mesh-heated vacuum furnace (CXZW-45-20, Shanghai Chenxin Electric Furnace Co., Ltd., China). After sintering, all the samples were annealed at 1400 ℃ for 10 h in air and mirror polished on both surfaces to a thickness of 0.6 mm for further characterization.

2.2 Characterization

Crystalline phases of the ceramics were collected by using a powder X-ray diffractometer (XRD; D8 Advance, Bruker, Germany) in the 2θ range from 15° to 70° with Cu Kα radiation (λ = 1.54056 Å) working at 40 kV and 30 mA. To characterize the microstructures, the polished CSS:Ce ceramics were thermally etched in air at 1450 ℃ for 3 h. Microstructure investigation was performed by a scanning electron microscope (SEM; Model S-4800, Hitachi, Japan). The average particle size or grain size was determined from SEM micrographs using the linear intercept technique by counting over 500 particles or grains. The bulk density of the sintered ceramics was determined by Archimedes method using distilled water as displacement liquid. Using the calculated lattice parameters, the theoretical density of fully dense CSS ceramics was taken to be 3.514 g/cm^3. PL and PLE spectra were recorded using a fluorescence spectrometer (F920, Edinburgh, UK). The fluorescence decay of the Ce^{3+} emission was measured using the time-correlated single-photon counting method on the F920 spectrometer equipped with a photon counting detector of a photomultiplier tube (PMT; R928, Hamamatsu Photonics, Japan) and a hydrogen flash lamp as an excitation source. A photoluminescence quantum efficiency spectrometer (Quantaurus-QY Plus C13534-12, Hamamatsu Photonics, Japan) was used to record external/internal quantum efficiency (EQE/IQE) and light absorption efficiency (AE). Temperature-dependent PL spectra were obtained by a home-built measurement system, which consists of a 450 nm blue LD, a fluorescence microscope (BX53M, Olympus, Japan), a cooling/heating stage (THMS-600, Linkam, UK), and a charge-coupled device (CCD) spectrometer (QEPro, Ocean Optics, China). The temperature was increased from 88 to 838 K with a step size of 50 K at a heating rate of 50 K/min, and the ceramics were held at each temperature for 2 min. The total transmittance spectrum of the ceramics ranging from 250 to 800 nm was conducted on a dual-beam spectrophotometer (UV-3600 plus, Shimadzu, Japan) equipped with an integrating sphere. Electroluminescence (EL) properties of the ceramics under blue LD excitation were measured in a 40-cm-diameter integrating sphere equipped with a spectrophotometric system using an integrated test system (HAAS-2000, EVERFINE, China). The optical power of the blue LD, as determined by the input current, was measured with a laser power meter (PM100D, THORLABS, USA). The laser spot was captured by a beam analyzer (BC106N-VIS, Thorlabs, USA), and the beam diameter was determined according to the International Organization for Standardization (ISO) 11146. The laser spot size was calculated to be 0.11 mm^2. The thermal conductivity of the CSS:Ce ceramics at 25 and 250 ℃ was measured by the transient hot disk method (TPS2500S, Hot Disk, Sweden). The surface temperature of the samples was measured by an infrared thermal imaging system (ETS320, FLIR, USA). All the measurements were conducted at room temperature unless specially mentioned.

3 Results and discussion

It is well known that both optical and thermal properties of the transparent ceramics are dependent on the final density and microstructure [38,53]. The sintering process commonly plays a crucial role in

controlled densification and microstructural evolution of the ceramics. It should be carefully designed to obtain transparent CSS:Ce ceramics. In our study, the TSS technique was adopted to realize the densification of CSS:Ce silicate ceramics. Figure 1(a) shows a micrograph of mixed ceramic powders. It is clear that raw materials were finely ground together by ball milling. The powders exhibit good dispersion and uniform size distribution ranging from 0.5 to 2.5 μm (Fig. S1 in the Electronic Supplementary Material (ESM)). Figure 1(b) shows the microstructure of the ceramics via single-step conventional sintering at 1450 ℃ for 10 h (denoted as 1450 ℃×10 h). The average grain size is ~2.5 μm, and its relative density reaches 97.5% (Table 1). Several coarse pores with sizes larger than 5 μm and many fine pores at triple junctions are observed. When single-step zero-time sintering was adopted (denoted as 1500 ℃×0 h), the ceramic exhibits a slightly finer grain size of ~1.6 μm with an improved relative density of 98.3% (Table 1), and no coarse pores are observed (Fig. 1(c)). However, it shows an inhomogeneous microstructure with an abnormal grain as large as ~10 μm. In contrast, the ceramics obtained by the TSS technique (denoted as 1500 ℃×0 h+1450℃×10 h) present a consolidated microstructure, and most of the fine pores at the triple junctions have been eliminated (Fig. 1(d)). The relative density reaches as high as 99.7% (Table 1). The average grain size is ~96 μm, which is much larger than that of the ceramics by single-step sintering. The results suggest that the TSS scheme is more effective in the densification of the CSS ceramics. To observe the microstructure evolution during the second stage, the CSS:Ce ceramics were first heated to 1500 ℃, then immediately cooled to 1450 ℃, and held for 6 h (denoted as 1500 ℃×0 h+1450 ℃×6 h). The microstructure shows a bimodal grain size distribution, where coarse grains (90 μm) are surrounded by fine grains (3.7 μm) (Fig. S2 in the ESM). The related mechanism is proposed as follows: The first-step sintering at 1500 ℃ involves a liquid-phase sintering process due to the sintering aids, which form a liquid phase once above 1500 ℃. The liquid can penetrate grain boundaries so that liquid films are formed. The liquid film permits easy grain sliding and grain fragmentation, which favours rapid densification and abnormal grain growth [54,55]. The second step at 1450 ℃ is solid-state sintering, in which abnormally large grains swallowed finer grains via grain boundary emigration (Fig. S2 in the ESM), and most pores were eliminated by grain boundary diffusion. The difference in the microstructure clearly demonstrates the advantage

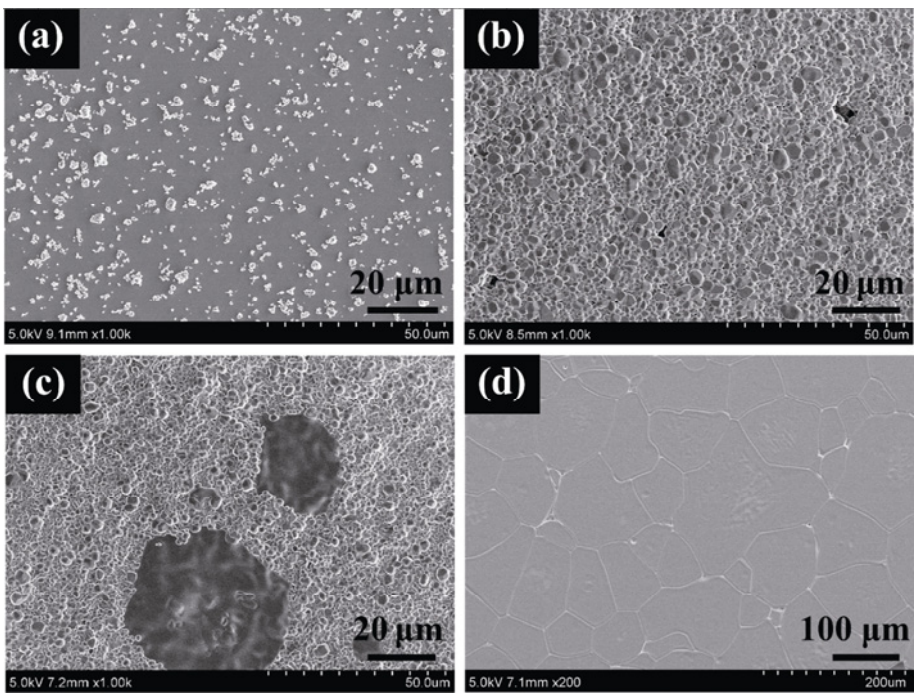

Fig. 1 SEM images of (a) mixed ceramic powders and thermally etched surface of CSS:0.5%Ce ceramics prepared by different heating schedules: (b) single-step sintering 1450 ℃×10 h, (c) single-step sintering 1500 ℃×0 h, and (d) two-step sintering (1500 ℃×0 h+1450 ℃×10 h).

Table 1 Density and relative density of CSS:Ce ceramics prepared by different heating schedules

Heating schedule	Density (g/cm^3)	Relative density (%)
Single-step sintering (1450 ℃×10 h)	3.427	97.5
Single-step sintering (1500 ℃×0 h)	3.454	98.3
Two-step sintering (1500 ℃×0 h+1450 ℃×10 h)	3.504	99.7

of TSS over other processing methods in obtaining the CSS:Ce transparent ceramics. In addition, the EDS line scan analysis is used to analyze the compositional variation between inner grains and grain boundaries. Ca, Sc, and Si contents remain steady across the grain boundary, indicating a uniform distribution of the elements (Fig. S3 in the ESM).

Figure 2(a) shows a transmittance spectrum of CSS:0.5%Ce transparent ceramics fabricated by TSS. It can be seen that the ceramics have high transparency, and the below letters "CSS" are clearly seen. In contrast, the mirror-polished ceramics by single-step sintering are opaque because of Rayleigh scattering from residual pores. Under 450 nm blue light, the ceramics exhibit an intense cyan-green emission. According to the transmittance spectrum, the highest transmittance is above 71% in the range of 500–800 nm. The absorption band of around 420–480 nm is assigned to the 4f→5d transition of Ce^{3+}. XRD patterns of the CSS:0.5%Ce transparent ceramics are shown in Fig. 2(b). The CSS host has a cubic garnet-type structure with the *Ia*3*d* space group (No. 230) [56]. All the diffraction peaks of the ceramics can be well indexed to the standard card of $Ca_3Sc_2Si_3O_{12}$ (ICSS No 72-1969). No traces of other phases or impurities are detected, indicating that a pure garnet crystalline phase of the CSS:Ce ceramics is obtained.

PLE and PL spectra of the CSS:0.5%Ce^{3+} transparent ceramics were investigated (Fig. S4 in the ESM, Fig. 3). The PLE spectrum exhibits two broad excitation bands peaking at 310 and 445 nm, attributed to the transitions from 4f to $5d_2$ and $5d_1$ levels of Ce^{3+}, respectively. The excitation band peaking at ~445 nm has a full width at half-maximum (FWHM) of ~70 nm. This board excitation band is of benefit for the CSS:Ce ceramics to absorb blue light. Thus the CSS:Ce ceramics are compatible with blue LD chips that have an emission light of 430–480 nm.

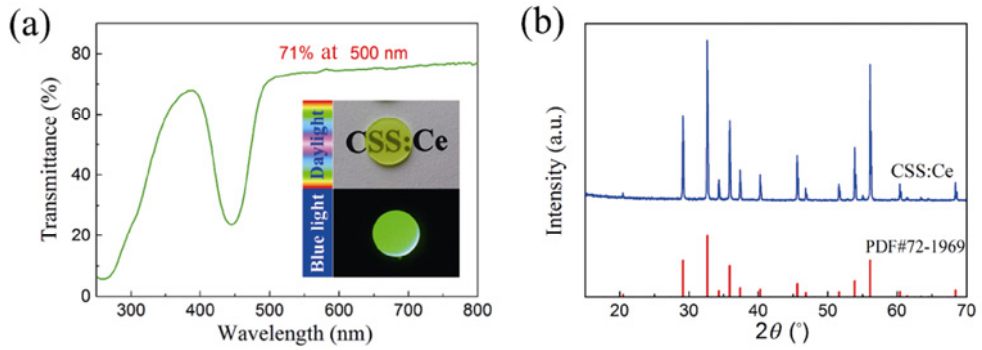

Fig. 2 (a) Transmittance spectrum of CSS:0.5%Ce transparent ceramics with a thickness of 0.6 mm. (b) XRD patterns of CSS:0.5%Ce transparent ceramics; the inset is photographs of ceramics under daylight and blue light.

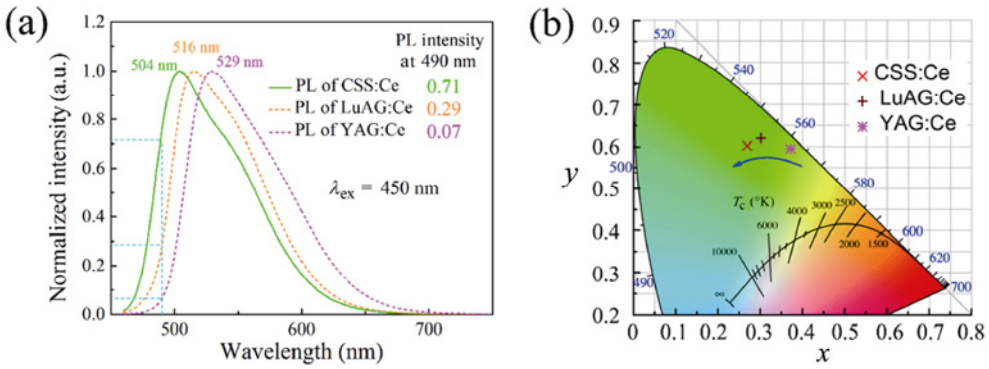

Fig. 3 (a) PL spectra of CSS:0.5%Ce, YAG:0.5%Ce, and LuAG:0.5%Ce transparent ceramics. (b) Emission colors in CIE-1931 chromaticity diagram.

Under blue light excitation (λ_{ex} = 450 nm), the CSS:0.5%Ce ceramics exhibit a broad cyan-green emission band with a peak at ~504 nm, arising from the 5d–4f transition of Ce^{3+} (Fig. 3(a)). Compared with the Ce^{3+} emission in LuAG:0.5%Ce ceramics (peaking at 517 nm) and YAG:0.5%Ce ceramics (peaking at 529 nm), the CSS:0.5%Ce ceramics have a more blue-shift emission. The PL intensity of the CSS:Ce ceramics at the typical cyan wavelength of 490 nm remains 71% of the emission peak intensity, while that of LuAG:Ce and YAG:Ce are only 29% and 7%, respectively. CSS:Ce has rich cyan-emitting components and can fill the aforementioned "cyan cavity" effectively. Based on the PL spectra, chromaticity coordinates for the ceramics are plotted on the CIE-1931 chromaticity diagram (Fig. 3(b)). The CIE color coordinates of CSS:Ce calculated between 480 and 720 nm were x = 0.30 and y = 0.59. IQE and EQE measurements were also implemented to lucubrate luminescence behavior. Under 450 nm excitation, IQE and EQE are as high as 91% and 62% (Fig. S5 in the ESM), respectively, which are higher than those of the reported LuAG:Ce and YAG:Ce ceramics [37,57]. To the best of our knowledge, the present CSS:Ce transparent ceramics are among the most efficient all-inorganic color converters by comparison with other transparent ceramics and single crystals.

Thermal stability is of vital importance for the color converters used in high-brightness laser lighting, as it determines reliability and efficiency of the whole device. Figure 5 presents the temperature-dependent PL spectra of the CSS:0.5%Ce ceramics under 0.2 W blue LD excitation. The integrated PL intensity is normalized to the value at 88 K. Obviously, the PL intensity declines gradually as the temperature increases due to the strengthened non-radiative relaxation. Below 588 K, the CSS:Ce ceramics exhibit similar thermal stability as the famous LuAG:0.5% ceramics. However, when the temperature is above 588 K, CSS:Ce exhibits much better thermal stability. The thermal quenching temperature ($T_{0.5}$) defined as the temperature at which the emission intensity is 50% of its original value is a parameter that characterizes luminescence thermal stability of phosphor materials. From Fig. 4(b), it can be obtained that $T_{0.5}$ of the CSS:Ce ceramics is 838 K, which is about 100 K higher than that of LuAG:Ce (738 K) [37]. The CSS:Ce ceramics exhibit excellent thermal stability, especially at high temperatures, due to the large energy separation between the Ce^{3+} $5d_1$ level and the conduction band (CB) of the CSS hosts. Larger $E_{5d1\text{-}CB}$ value means that the electron at the Ce^{3+} $5d_1$ level requires more thermal energy (higher temperature) to be promoted into CB of the host, followed by charge trapping (luminescence quenching) at defects [51]. Thermal conductivity of the color converters is another important parameter for laser lighting, because if the huge amount of heat generated during operation cannot be dissipated quickly, it will give rise to thermal quenching of the color converters. The CSS:0.5%Ce ceramics have thermal conductivity of 6.1 and 4.2 W/(m·K) at 25 and 250 ℃, respectively, which is comparable to that of the LuAG:Ce ceramics [37]. Such thermally stable emission and high thermal conductivity of the CSS:Ce ceramics provide a great promise for high-brightness laser lighting devices.

The PL spectra of CSS:$x$$Ce^{3+}$($x$ = 0.3%–0.9%) transparent ceramics with different Ce^{3+} concentrations are depicted in Fig. 5(a). It can be seen that the PL intensity of the CSS:Ce ceramics increases with the increasing Ce^{3+} concentration. Note that the emission peak gradually shifts from 503 to 506 nm with the Ce^{3+} concentration increasing from 0.3% to 0.9% (Fig. S6 in

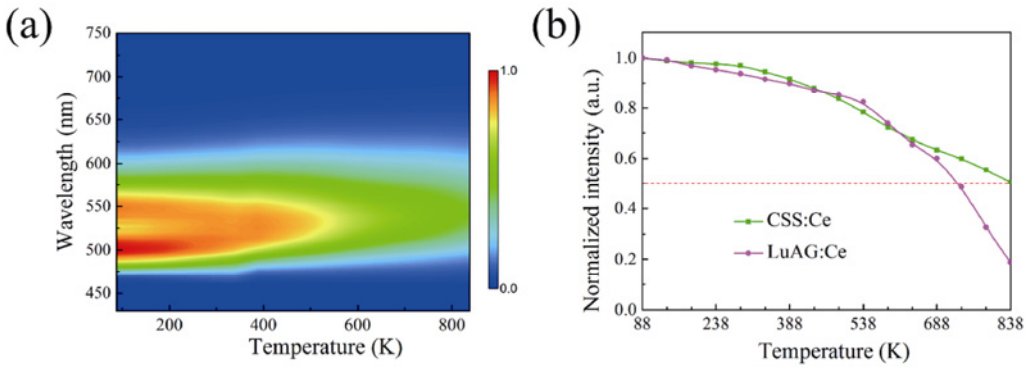

Fig. 4 (a) Temperature-dependent PL spectra of CSS:0.5%Ce transparent ceramics. (b) Normalized integrated PL intensitiy of CSS:0.5%Ce and LuAG:0.5%Ce transparent ceramics.

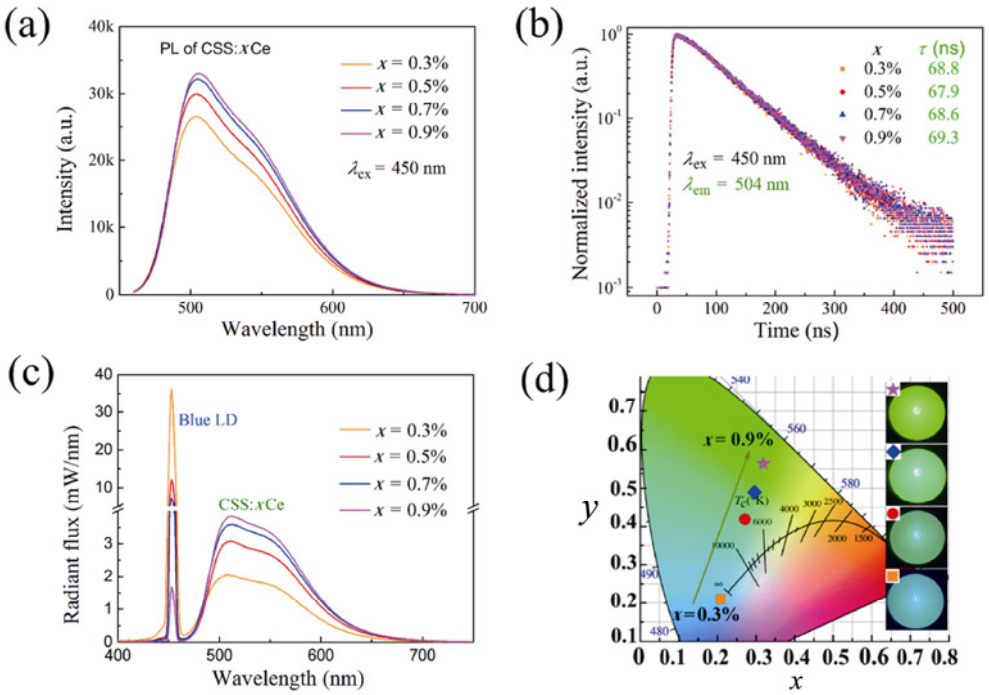

Fig. 5 (a) PL spectra, (b) fluorescence decay curves, (c) EL spectra under excitation of 0.72 W blue laser, and (d) corresponding color coordinates of CSS:*x*Ce transparent ceramics with a thickness of 0.6 mm; the insets are corresponding luminescence photographs.

the ESM). This redshift should be attributed to strengthened crystal-field splitting because of the replacement of smaller Ca^{2+} by the larger Ce^{3+} and the reabsorption between Ce^{3+} ions [58]. Figure 5(b) shows fluorescence decay curves of the emission monitored at 504 nm for different Ce^{3+} concentrations. The decay curves are almost insusceptible to the variation of the Ce^{3+} concentration from 0.3% to 0.9%, indicating that the nonradiative relaxation due to the interaction among the Ce^{3+} ions can be ignored for the Ce^{3+} concentration $\leqslant$ 0.9%. All the curves can be well-fitted with a single-exponential function. The average lifetime of CSS:*x*Ce (x = 0.3%–0.9%) is ~68.7 ns, comparable to that of LuAG:0.5%Ce (57.1 ns) and YAG:0.5%Ce ceramics (61.3 ns) (Fig. S7 in the ESM).

Since ultimate goal of this work is to develop ceramic materials as the color converters for blue LD pumped high-brightness lighting systems, the luminous performance of the CSS:Ce ceramics in practical laser-based lighting was thus evaluated. Similar to our previous report [41], the measurement was conducted in a transmissive configuration equipped with a 450 nm blue LD, as shown in Fig. 6(a). Because of spontaneous emission characteristics of the phosphor ceramics, phosphor-converted cyan-green light is isotropically scattered in all directions, and only the forward scattered light is collected for illumination in our study. Upon carefully balancing the mechanical strength, size, and raw material cost, the thickness of the transparent ceramics was fixed at ~0.6 mm. The Ce^{3+} concentration was then optimized by measuring EL of different ceramics under a 0.73 W blue laser, as shown in Fig. 5(c). Each EL spectrum is composed of two emission bands: A sharp blue band from the transmitted blue laser and a broad cyan-green band in the range of 480–720 nm from the CSS:Ce ceramics. As the Ce^{3+} concentration increases, the transmitted blue light decreases gradually, and the forward converted cyan-green light increases simultaneously. As shown in Fig. 5(d), the CIE color coordinate of the constructed white laser lighting shifts from blue to pale-cyan and finally to green due to the increasing cyan-green emission component, which is in accordance with their luminescence photographs. The optimal Ce^{3+} concentration is then elected as 0.5% by considering the appropriate balance between blue and cyan-green emission for white light generation.

The CSS:0.5%Ce transparent ceramics with a thickness of 0.6 mm were chosen for further investigation. The laser spot size was measured to be 0.11 mm^2. As shown in Fig. 6(b), the cyan-green emission intensity increases monotonously with the

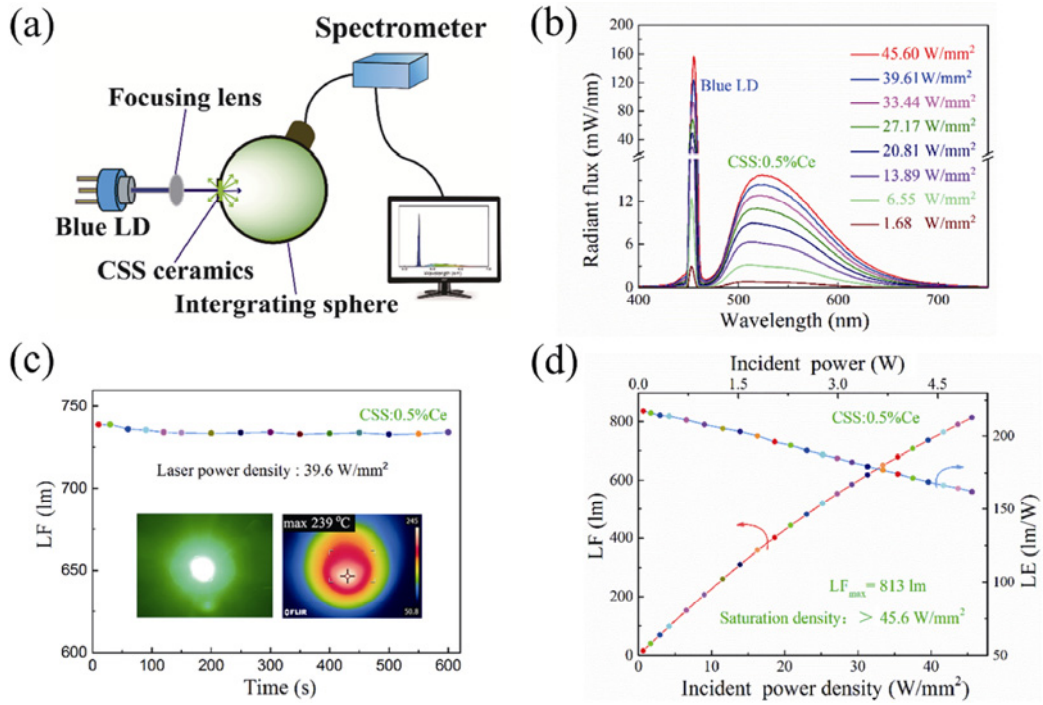

Fig. 6 (a) Schematic illustration of measurement device in transmissive configuration. (b) Forward EL spectra of CSS:0.5%Ce transparent ceramics constructed laser devices under various laser power density excitation. (c) Forward LF variation under continuous 39.6 W/mm^2 laser excitation. (d) Forward LF and LE as a function of incident laser power density; the insert illustrates corresponding lighting photographs and thermal infrared images.

increasing incident laser power density, and the luminescence saturation does not occur. The CSS:Ce ceramics could withstand high incident laser power density of 45.6 W/mm^2 and yields a maximum forward luminous flux (LF) of 813 lm. As to the luminous efficacy (LE), however, it decreases steadily with the increasing incident laser power density due to the decreased blue light absorption coefficient and strengthened thermal quenching. The forward LE amounts to 211 lm/W under the excitation of the blue laser of 6.6 W/mm^2, which is comparable to that of the LuAG:Ce ceramics [37]. It decreases to 162 lm/W when increasing the incident laser density to 45.6 W/mm^2. The output LF and LE can be further enhanced by designing a secondary optic to reuse the backward scattering light [21,59]. Under continuous laser irradiation of 39.6 W/mm^2 and in the absence of heat sink, the CSS:Ce ceramics could operate efficiently and reliably without luminescence degradation, and the corresponding surface temperature is ~239 ℃ (Fig. 6(c)). The CSS:Ce ceramics have an extremely high saturation threshold of up to 45.6 W/mm^2 due to (i) high thermal stability and (ii) low heat generation as a result of high efficiency and small Stokes shift in the color conversion process. It is worthy to mention that for the same volume (e.g., 5 mm × 5 mm × 0.6 mm) of CSS:Ce and LuAG:Ce transparent ceramics, the amount of expensive Sc_2O_3 raw materials used in the CSS:Ce ceramics (14.96 mg) is much lower than that of equally expensive Lu_2O_3 used in the LuAG:Ce ceramics (70.76 mg). Considering the cost-effective raw materials and low-temperature preparation technology (less energy consumption), the CSS:Ce transparent ceramics are thus economically attractive while maintaining similar or even better optical properties than the conventional LuAG:Ce transparent ceramics.

4 Conclusions

In summary, for the first time, efficient and thermally robust cyan-green emitting CSS:Ce transparent ceramics have been successfully fabricated by adapting a TSS method. The completely densified ceramics exhibit high optical transmittance of 71%. Under 450 nm excitation, the ceramics exhibit an efficient cyan-green emission band peaking at 504 nm, and the corresponding IQE and EQE are as high as 91% and 62%. Furthermore, it features a high thermal quenching temperature of up to 838 K, 100 K higher

than that of the LuAG:Ce ceramics (738 K). Under the excitation of the blue LD of 45.6 W/mm^2, the CSS:Ce ceramics yield cyan-green light with forward LF of 813 lm and forward LE of 162 lm/W. These results demonstrate that the CSS:Ce transparent ceramics could be an excellent cyan-green color converter for high-brightness laser lighting.

Acknowledgements

This work was partially supported by National Natural Science Foundation of China (Grant Nos. U22A20139, 52102192, 51772286, 11974346, 12074373, 52072361, and 12074374), National Key R&D Program of China (Grant No. 2021YFB3502701), Youth Innovation Promotion Association CAS (Grant No. 2020222), Key Research and Development Program of Jilin Province (Grant Nos. 20210201024GX, 20220101208JC, and 20230101123JC), Changchun Science and Technology Planning Project (Grant No. 21ZGY05), and the Opening Project Key Laboratory of Transparent Opto-functional Inorganic Material, Chinese Academy of Sciences.

Declaration of competing interest

The authors have no competing interests to declare that are relevant to the content of this article.

Electronic Supplementary Material

Supplementary material is available in the online version of this article at https://doi.org/10.26599/JAC.2023.9220782.

References

[1] Li SX, Wang L, Hirosaki N, *et al*. Color conversion materials for high-brightness laser-driven solid-state lighting. *Laser Photonics Rev* 2018, **12**: 1800173.

[2] Li XF, Budai JD, Liu F, *et al*. New yellow $Ba_{0.93}Eu_{0.07}Al_2O_4$ phosphor for warm-white light-emitting diodes through single-emitting-center conversion. *Light Sci Appl* 2013, **2**: e50.

[3] Lin H, Hu T, Cheng Y, *et al*. Glass ceramic phosphors: Towards long-lifetime high-power white light-emitting-diode applications—A review. *Laser Photonics Rev* 2018, **12**: 1700344.

[4] Hye Oh J, Yang SJ, Rag Do Y. Healthy, natural, efficient and tunable lighting: Four-package white LEDs for optimizing the circadian effect, color quality and vision performance. *Light Sci Appl* 2014, **3**: e141.

[5] Li SX, Guo YQ, Xie RJ. Laser phosphors for next-generation lighting applications. *Acc Mater Res* 2022, **3**: 1299–1308.

[6] Xia ZG, Meijerink A. Ce^{3+}-doped garnet phosphors: Composition modification, luminescence properties and applications. *Chem Soc Rev* 2017, **46**: 275–299.

[7] Wang L, Xie RJ, Li YQ, *et al*. $Ca_{1-x}Li_xAl_{1-x}Si_{1+x}N_3:Eu^{2+}$ solid solutions as broadband, color-tunable and thermally robust red phosphors for superior color rendition white light-emitting diodes. *Light Sci Appl* 2016, **5**: e16155.

[8] Wei Y, Xing GC, Liu K, *et al*. New strategy for designing orangish-red-emitting phosphor via oxygen-vacancy-induced electronic localization. *Light Sci Appl* 2019, **8**: 15.

[9] Zhang D, Xiao WG, Liu C, *et al*. Highly efficient phosphor-glass composites by pressureless sintering. *Nat Commun* 2020, **11**: 2805.

[10] Wu HJ, Hao ZD, Pan GH, *et al*. Phosphor–SiO_2 composite films suitable for white laser lighting with excellent color rendering. *J Eur Ceram Soc* 2020, **40**: 2439–2444.

[11] Peng Y, Yu ZK, Zhao JZ, *et al*. Unique sandwich design of high-efficiency heat-conducting phosphor-in-glass film for high-quality laser-driven white lighting. *J Adv Ceram* 2022, **11**: 1889–1900.

[12] Cantore M, Pfaff N, Farrell RM, *et al*. High luminous flux from single crystal phosphor-converted laser-based white lighting system. *Opt Express* 2016, **24**: A215–A221.

[13] Liu X, Qian XL, Zheng P, *et al*. Composition and structure design of three-layered composite phosphors for high color rendering chip-on-board light-emitting diode devices. *J Adv Ceram* 2021, **10**: 729–740.

[14] Huang QG, Lin H, Wang B, *et al*. Patterned glass ceramic design for high-brightness high-color-quality laser-driven lightings. *J Adv Ceram* 2022, **11**: 862–873.

[15] Lin SS, Lin H, Huang QM, *et al*. Highly crystalline $Y_3Al_5O_{12}:Ce^{3+}$ phosphor-in-glass film: A new composite color converter for next-generation high-brightness laser-driven lightings. *Laser Photonics Rev* 2022, **16**: 2200523.

[16] Huang QG, Sui P, Huang F, *et al*. Toward high-quality laser-driven lightings: Chromaticity-tunable phosphor-in-glass film with "phosphor pattern" design. *Laser Photonics Rev* 2022, **16**: 2200040.

[17] Lin T, Chen HX, Li SX, *et al*. Bi-color phosphor-in-glass films achieve superior color quality laser-driven stage spotlights. *Chem Eng J* 2022, **444**: 136591.

[18] Ling JR, Zhou YF, Xu WT, *et al*. Red-emitting YAG:Ce, Mn transparent ceramics for warm WLEDs application. *J Adv Ceram* 2020, **9**: 45–54.

[19] Zheng GJ, Xiao WG, Wu HJ, *et al*. Far-red-emitting ceramics: Near-unity and zero-thermal-quenching far-red-emitting composite ceramics via pressureless glass crystallization. *Laser Photonics Rev* 2021, **15**: 2170038.

[20] Zhou TY, Hou C, Zhang L, *et al*. Efficient spectral regulation in $Ce:Lu_3(Al,Cr)_5O_{12}$ and $Ce:Lu_3(Al,Cr)_5O_{12}$/$Ce:Y_3Al_5O_{12}$ transparent ceramics with high color rendering

index for high-power white LEDs/LDs. *J Adv Ceram* 2021, **10**: 1107–1118.

[21] Zheng P, Li SX, Wang L, *et al*. Unique color converter architecture enabling phosphor-in-glass (PiG) films suitable for high-power and high-luminance laser-driven white lighting. *ACS Appl Mater Interfaces* 2018, **10**: 14930–14940.

[22] Cheng ZQ, Liu X, Chen XR, *et al*. Composition and luminescence properties of highly robust green-emitting LuAG:Ce/Al_2O_3 composite phosphor ceramics for high-power solid-state lighting. *J Adv Ceram* 2023, **12**: 625–633.

[23] Yang ZZ, Zheng S, Pang T, *et al*. YAG:Ce PiGF@alumina-substrate in a reflection mode for high-brightness laser-driven projection display. *Adv Mater Technol* 2023: 2300132.

[24] Li SX, Zhu QQ, Tang DM, *et al*. Al_2O_3–YAG:Ce composite phosphor ceramic: A thermally robust and efficient color converter for solid state laser lighting. *J Mater Chem C* 2016, **4**: 8648–8654.

[25] Huang P, Zhou BY, Zheng Q, *et al*. Nano wave plates structuring and index matching in transparent hydroxyapatite-YAG:Ce composite ceramics for high luminous efficiency white light-emitting diodes. *Adv Mater* 2020, **32**: e1905951.

[26] Wang JC, Tang XY, Zheng P, *et al*. Thermally self-managing YAG:Ce–Al_2O_3 color converters enabling high-brightness laser-driven solid state lighting in a transmissive configuration. *J Mater Chem C* 2019, **7**: 3901–3908.

[27] Xu YR, Li SX, Zheng P, *et al*. A search for extra-high brightness laser-driven color converters by investigating thermally-induced luminance saturation. *J Mater Chem C* 2019, **7**: 11449–11456.

[28] Nishiura S, Tanabe S, Fujioka K, *et al*. Properties of transparent Ce:YAG ceramic phosphors for white LED. *Opt Mater* 2011, **33**: 688–691.

[29] Liu S, Sun P, Liu YF, *et al*. Warm white light with a high color-rendering index from a single $Gd_3Al_4GaO_{12}:Ce^{3+}$ transparent ceramic for high-power LEDs and LDs. *ACS Appl Mater Interfaces* 2019, **11**: 2130–2139.

[30] Liu X, Zhou HY, Hu ZW, *et al*. Transparent Ce:GdYAG ceramic color converters for high-brightness white LEDs and LDs. *Opt Mater* 2019, **88**: 97–102.

[31] Yao Q, Hu P, Sun P, *et al*. YAG:Ce^{3+} transparent ceramic phosphors brighten the next-generation laser-driven lighting. *Adv Mater* 2020, **32**: e1907888.

[32] Ma YL, Zhang L, Zhou TY, *et al*. Weak thermal quenching and tunable luminescence in Ce:$Y_3(Al,Sc)_5O_{12}$ transparent ceramics for high power white LEDs/LDs. *Chem Eng J* 2020, **398**: 125486.

[33] Li SX, Zhu QQ, Wang L, *et al*. $CaAlSiN_3:Eu^{2+}$ translucent ceramic: A promising robust and efficient red color converter for solid state laser displays and lighting. *J Mater Chem C* 2016, **4**: 8197–8205.

[34] Hu T, Ning LX, Gao Y, *et al*. Glass crystallization making red phosphor for high-power warm white lighting. *Light Sci Appl* 2021, **10**: 56.

[35] Osborne RA, Cherepy NJ, Seeley ZM, *et al*. New red phosphor ceramic $K_2SiF_6:Mn^{4+}$. *Opt Mater* 2020, **107**: 110140.

[36] Lee JW, Cha JM, Bae BH, *et al*. Effects of using MgO, CaO additives as sintering aid in pressureless sintering of $M_2Si_5N_8:Eu^{2+}$ (M = Ba, Sr) phosphor ceramics for amber LED automotive applications. *J Alloys Compd* 2021, **858**: 157710.

[37] Ding H, Liu ZH, Hu P, *et al*. High efficiency green-emitting LuAG:Ce ceramic phosphors for laser diode lighting. *Adv Optical Mater* 2021, **9**: 2002141.

[38] Zhang YL, Hu S, Wang ZJ, *et al*. Pore-existing $Lu_3Al_5O_{12}$:Ce ceramic phosphor: An efficient green color converter for laser light source. *J Lumin* 2018, **197**: 331–334.

[39] Hua H, Feng SW, Ouyang ZY, *et al*. YAGG:Ce transparent ceramics with high luminous efficiency for solid-state lighting application. *J Adv Ceram* 2019, **8**: 389–398.

[40] Zhao M, Liao HX, Molokeev MS, *et al*. Emerging ultra-narrow-band cyan-emitting phosphor for white LEDs with enhanced color rendition. *Light Sci Appl* 2019, **8**: 38.

[41] Wu HJ, Pan GH, Hao ZD, *et al*. Highly efficient and thermally robust cyan-green phosphor-in-glass films for high-brightness laser lighting. *J Mater Chem C* 2021, **9**: 12342–12352.

[42] Zhu QQ, Meng Y, Zhang H, *et al*. YAGG: Ce phosphor-in-YAG ceramic: An efficient green color converter suitable for high-power blue laser lighting. *ACS Appl Electron Mater* 2020, **2**: 2644–2650.

[43] Ling JR, Xu WT, Yang J, *et al*. The effect of Lu^{3+} doping upon YAG:Ce phosphor ceramics for high-power white LEDs. *J Eur Ceram Soc* 2021, **41**: 5967–5976.

[44] Huang S, Shang MM, Yan Y, *et al*. Ultra-broadband green-emitting phosphors without cyan gap based on double-heterovalent substitution strategy for full-spectrum WLED lighting. *Laser Photonics Rev* 2022, **16**: 2200473.

[45] Wang PF, Lin H, Lin SS, *et al*. Reducing the cyan-cavity: $Lu_2MAl_4SiO_{12}:Ce^{3+}$ (M = Mg, Ca, Sr and Ba) phosphor-in-glass film towards full-spectrum laser-driven lighting. *J Mater Chem C* 2022, **10**: 16337–16346.

[46] Yuan WH, Pang R, Wang SW, *et al*. Enhanced blue-light excited cyan-emitting persistent luminescence of $BaLu_2Al_2Ga_2SiO_{12}:Ce^{3+},Bi^{3+}$ phosphors for AC-LEDs via defect modulation. *Light Sci Appl* 2022, **11**: 184.

[47] Liu YF, Zhang X, Hao ZD, *et al*. Crystal structure and luminescence properties of $(Ca_{2.94-x}Lu_xCe_{0.06})(Sc_{2-y}Mg_y)Si_3O_{12}$ phosphors for white LEDs with excellent colour rendering and high luminous efficiency. *J Phys D*: *Appl Phys* 2011, **44**: 075402.

[48] Liu YF, Zhang X, Hao ZD, *et al*. Generation of broadband emission by incorporating N^{3-} into $Ca_3Sc_2Si_3O_{12}:Ce^{3+}$ garnet for high rendering white LEDs. *J Mater Chem* 2011, **21**: 6354–6358.

[49] Shimomura Y, Honma T, Shigeiwa M, *et al*. Photoluminescence and crystal structure of green-emitting $Ca_3Sc_2Si_3O_{12}:Ce^{3+}$ phosphor for white light emitting diodes. *J Electrochem Soc* 2007, **154**: J35.

[50] Liu YF, Zhang X, Hao ZD, *et al*. Tunable full-color-emitting $Ca_3Sc_2Si_3O_{12}:Ce^{3+}$, Mn^{2+} phosphor via charge compensation and energy transfer. *Chem Commun* 2011, **47**: 10677–10679.

[51] Sharma SK, Lin YC, Carrasco I, *et al*. Weak thermal quenching of the luminescence in the $Ca_3Sc_2Si_3O_{12}:Ce^{3+}$ garnet phosphor. *J Mater Chem C* 2018, **6**: 8923–8933.

[52] Irifune T, Kawakami K, Arimoto T, *et al*. Pressure-induced nano-crystallization of silicate garnets from glass. *Nat Commun* 2016, **7**: 13753.

[53] Zheng P, Li SX, Wei R, *et al*. Unique design strategy for laser-driven color converters enabling superhigh-luminance and high-directionality white light. *Laser Photonics Rev* 2019, **13**: 1900147.

[54] Kang SJ L, Kim KH, Yoon DN. Densification and shrinkage during liquid-phase sintering. *J Am Ceram Soc* 1991, **74**: 425–427.

[55] Liu YX, Tandon R, German RM. Modeling of supersolidus liquid phase sintering: II. Densification. *Metall Mater Trans A* 1995, **26**: 2423–2430.

[56] Jia ZW, Yuan CX, Liu YF, *et al*. Strategies to approach high performance in Cr^{3+}-doped phosphors for high-power NIR-LED light sources. *Light Sci Appl* 2020, **9**: 86.

[57] Ding H, Hu P, Liu ZH, *et al*. Effect of Ca^{2+}–Si^{4+} on $Y_3Al_5O_{12}$:Ce ceramic phosphors for white laser-diodes lighting. *Appl Phys Lett* 2021, **118**: 211902.

[58] Sun P, Hu P, Liu YF, *et al*. Broadband emissions from $Lu_2Mg_2Al_2Si_2O_{12}:Ce^{3+}$ plate ceramic phosphors enable a high color-rendering index for laser-driven lighting. *J Mater Chem C* 2020, **8**: 1405–1412.

[59] Ma YP, Luo XB. Small-divergent-angle uniform illumination with enhanced luminance of transmissive phosphor-converted white laser diode by secondary optics design. *Opt Lasers Eng* 2019, **122**: 14–22.